ACS Catalysis

Research Article

pubs.acs.org/acscatalysis

Enhanced Oxygen Reduction Reaction Activity Due to Electronic Effects between Ag and Mn_3O_4 in Alkaline Media

Shin-Ae Park,[†] Hankwon Lim,[‡] and Yong-Tae Kim*[,†]

[†]School of Mechanical Engineering, Pusan National University, Busan 609-735, Republic of Korea

[‡]Department of Chemical Systematic Engineering, Catholic University of Daegu, Daegu 712-702, Republic of Korea

Supporting Information

ABSTRACT: Ag is considered to be among the most promising electrocatalysts for the oxygen reduction reaction (ORR) in alkaline media and is suitable for application in various electrochemical energy devices such as metal−air batteries and alkaline fuel cells. In this study, we studied the role of the electronic effects induced by strong metal support interactions in Ag/Mn_3O_4/C in enhancing the ORR activity in alkaline media. Ag supported on Mn_3O_4 showed a much higher ORR activity than Ag supported on carbon, and an upshift in the d-band center was observed in the former case, due to charge transfer from Ag to Mn. Further, the strain effect observed by X-ray absorption fine structure analysis, induced an increase in the O−O bond split kinetics due to upshift of the d-band center, resulting in enhanced ORR activity on Ag/Mn_3O_4/C. In conclusion, we propose that in-depth consideration of electronic effects is essential when designing metal/metal oxide catalysts for the ORR in alkaline media.

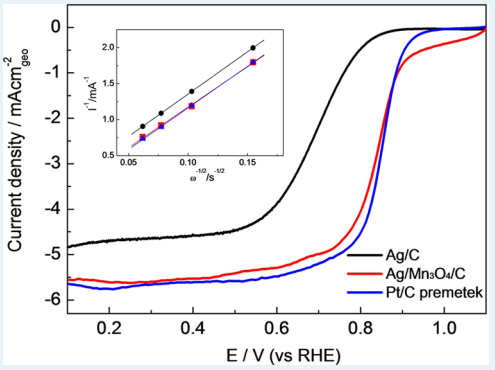

KEYWORDS: *oxygen reduction reaction, strong metal support interaction (SMSI), ligand effect, strain effect, d-band center, silver*

INTRODUCTION

Recently, much attention has been paid to electrochemical catalysts that promote oxygen reduction reaction (ORR) in the alkaline media, because this reaction tends to be the rate-determining step in various electrochemical energy storage and conversion devices that use alkaline electrolytes such as metal−air batteries and alkaline fuel cells.[1] Research efforts over the past few years have been focused on developing non-Pt materials such as Ag,[2,3] Au,[4,5] Pd,[6,7] Ni,[8] manganese oxide,[9,10] spinels,[11] perovskites,[12] and metal oxides on graphene,[13−16] because fast ORR is observed in alkaline media compared to the acidic media. Among these materials, Ag is regarded as a promising material, owing to its high ORR activity and low cost. So far, various methods have been adopted to enhance the activity of Ag such as size control,[17,18] alloying with Pd (AgPd),[19] and compositing with metal oxides (e.g., Ag/TiO_2, Ag/Mn_3O_4/C).[20−22] Among these methods, compositing with metal oxides has been studied the most, to enhance the ORR activity.[20,21]

In general, metal/metal oxide composites are known to exhibit strong metal support interactions (SMSIs), which induce a change in the ORR activity due to the strain effect. Most of the studies have focused on the SMSI of catalysts in acidic media (e.g., Pt/TiO_2).[23,24] Although various metal/metal oxide composites such as Pt/$CaMnO_3$, Pd/TiO_2, Pt/Ta_2O_5, Au/TiO_2, and Ag/TiO_2 have been studied in the alkaline media, the change in the ORR activity has been mainly attributed to the synergetic effect.[22,25−29] Even though the electrochemical mechanism for the enhancement in the ORR activity has been analyzed in terms of the bifunctional effect,[20,26] few studies on the effect of the catalyst properties on the ORR activity in alkaline media have been carried out.

Adzic et al. reported the difference in the ORR activities of various catalyst materials in the alkaline media in terms of the O−O bond breakage tendency and adsorption strength of O_2, which depend on the d-band center of the metal.[30] Metals with high d-band centers such as Ru, Ir, Rh, and Pd exhibit low ORR activity because of the difficult desorption of oxygenated intermediates, even when the O−O bonds are broken easily. The difficult desorption is a result of the higher adsorption strength of O_2. On the other hand, metals with a low d-band center such as Ag and Au have low ORR activity, owing to the slow kinetics of the O−O bond split even though O_2 adsorption is sufficiently weak. Therefore, an optimum balance between the O−O bond breaking kinetics and electroreduction of the oxygenated intermediates is believed to be key for maximizing the ORR activity of a catalyst. In other words, the electronic effect plays an important role in inducing a change in the ORR activity of metals, both in the alkaline media as well as in the acidic media.

In this study, we have extensively investigated the change in the O−O bond breakage, owing to the electronic effect of the SMSI of Ag/Mn_3O_4/C. Ag/Mn_3O_4/C, which is a metal/metal oxide composite catalyst, shows high ORR activity. The

Received: March 9, 2015
Revised: May 26, 2015
Published: May 26, 2015

DOI: 10.1021/acscatal.5b00495
ACS Catal. 2015, 5, 3995−4002

influence of the ligand and strain effects on the change in the d-band center, which affects the ORR activity, was investigated. The morphology and crystal structure of Ag/Mn_3O_4/C were observed by transmission electron microscopy (TEM) and X-ray diffraction (XRD), respectively. Electrochemical methods such as rotating disk electrode (RDE) and cyclic voltammetry (CV) were employed to evaluate the ORR activity in the alkaline media. X-ray photoelectron spectroscopy (XPS), X-ray absorption near edge structure (XANES) analysis, and density functional theory (DFT) calculations were used to examine the change in the electronic structure of Ag and Mn, to examine the ligand effect. Finally, the strain induced by Ag loaded in Mn_3O_4/C (Mn_3O_4 loaded on carbon) was evaluated from the extended X-ray absorption fine structure (EXAFS) data obtained from synchrotron facilities.

EXPERIMENTAL SECTION

Synthesis. Mn_3O_4/C particles were synthesized using a method previously reported in the literature.[21] $KMnO_4$ (1 g, ≥99%, Sigma-Aldrich) and vulcan carbon (0.1 g, XC-72) were added to deionized (DI) water (100 mL) and the solution was stirred for over 2 h at 80 °C, to fully dissolve the metal source in the solution. The solution was then evaporated in a vacuum evaporator, and dried at 80 °C in an oven for 24 h. The precursor obtained by this procedure was annealed at 400 °C for 2 h in a N_2 atmosphere to form Mn_3O_4/C. After the heat treatment, the Mn_3O_4/C powder was washed with DI water, dehydrated using a centrifuge, and dried at 80 °C in an oven to yield the final product. Ag (40 wt %) was loaded on the Mn_3O_4/C particles using the citrate-protecting method.[31] $AgNO_3$ (0.127 g, 99.9+%, Alfa Aesar) and sodium citrate (0.5 g, 99%, Alfa Aesar) were dissolved in DI water (100 mL). $NaBH_4$ (0.01 g) was also dissolved separately in DI water (10 mL). The $NaBH_4$ solution was then added dropwise to the $AgNO_3$/sodium citrate solution with vigorous stirring, to obtain a yellowish-brown Ag colloid. Subsequently, Mn_3O_4/C (0.12 g) was dispersed in DI water (50 mL), and the dispersion was ultrasonicated for 1 h. The mixture was added to the Ag colloid as the support. After allowing the mixture to rest for 1 day, the suspension was filtered, washed with copious amounts of DI water, and dried in an oven at 60 °C. Ag/C particles were synthesized using the same method as Ag/Mn_3O_4/C.

Characterization. The morphology of the powder was observed with STEM (Jem 2011) in the Korea Basic Science Institute (KBSI). Powder XRD analysis was performed with an Advance X-ray diffractometer (D8 ADVANCE) with Cu Kα radiation (λ = 1.54056 Å). X-ray diffraction data was collected over the 2θ range 20−90° with a step size of 0.02° and counting time of 0.2 s per step. XPS analysis was performed with 8A1 beamline at the Pohang Light Source (PLS). EXAFS data at the Mn *k*-edge and Ag *k*-edge were obtained in the transmission mode with synchrotron radiation (10C beamline, Pohang Light Source (PLS)) at room temperature. The spectra were processed using the program IFEFFIT[32−35] (version 1.2.11, IFEFFIT, Copyright 2008, Matthew Newville, University of Chicago, http://cars9.uchicago.edu/ifeffit/) with background subtraction (AUTOBK) and normalization. Fourier transformations of the EXAFS spectra were performed in the range of 2.5−12 Å in *k*-space and 1−3.25 Å in *R*-space with first-shell single scattering paths and k^3 weighting.

Electrochemical Measurements. For preparing the working electrode, Ag/Mn_3O_4/C (10 mg), Ag/C (10 mg), and Pt/C premetek (2.5 mg) were mixed with an RDE solution (2 mL) respectively, using a method reported previously.[36,37] After the solution was homogenized by sonication, 20 μL of the ink was drop-cast onto a glassy carbon electrode and then evaporated at room temperature to form a thin catalyst film. RDE measurements were performed in a three-electrode electrochemical cell with a potentiostat (Biologic VSP) at room temperature. The catalyst film-coated glassy carbon disk (AFE3T050GC, Pine; area: 0.19625 cm^2) was employed as the working electrode, whereas a Pt wire and mercury/mercury oxide (Hg/HgO) electrode were used as the counter and reference electrodes, respectively. CV measurements were performed in an nitrogen-saturated and oxygen-saturated 0.1 M KOH aqueous solution at a scan rate of 20 mV s^{-1}. ORR measurements were performed in an oxygen-saturated 0.1 M KOH aqueous solution with rotation rates of 100, 400, 900, 1600, and 2500 rpm at a scan rate of 10 mV s^{-1}. The rotating ring-disk electrode (RRDE) measurements were performed at room temperature. The working electrode (AFE7R9GCPT, Pine) was a catalyst-film-covered glassy carbon disk (0.2475 cm^2 in area), and the ring electrode was polycrystalline Pt (0.1866 cm^2 in area). The collection efficiency of the RRDE was N = 0.38, and the potential of the ring electrode was held at 1.22 V during the RRDE measurements.

Calculations. In this work, the DFT calculations were performed using the Cambridge Sequential Total Energy Package (CASTEP) code of Materials Studio.[38] Plane-wave expansion of the wave functions, and Vanderbilt-type ultrasoft pseudopotential formalism were employed.[39] We used the exchange-correlation functional based on the generalized gradient approximation (GGA) in the Perdew−Burke−Eruzerhof (PBE) scheme. In our calculations, Mn_3O_4 had an I41/amdS structure (space group No. 141), and the tetragonal unit cell containing 34 atoms was relaxed. We also added five Ag atoms on the (211) surface of Mn_3O_4 to perform calculations on Ag/Mn_3O_4. The Ag 4d 5s, Mn 3d 4s, and O 2s2p electrons were treated as the valence states. The plane-wave cutoff energy was 380 eV, and convergence was achieved with a (3 × 5 × 2) *k*-point mesh.

RESULTS

Morphological and Structural Characteristics. The morphology of Ag supported on Mn_3O_4/C and carbon was observed with TEM as shown in Figure 1. In the TEM images,

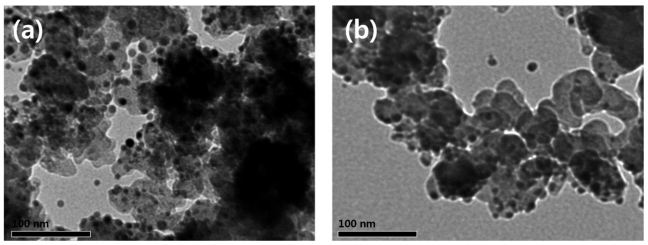

Figure 1. TEM micrographs of (a) Ag/Mn_3O_4/C and (b) Ag/C.

the dark-colored spheres are Ag particles, whereas the light-colored and bigger spheres are the supports (Mn_3O_4/C and carbon). Ag particles were dispersed evenly on the supports similar to the observations in the previous study.[18] It is well-known that the dispersion of catalyst particles depends on two steps, namely the synthesis of Ag colloidal particles and the supporting process. Since the average particle size of Ag in the composite with Mn_3O_4/C and carbon supports is approx-

DOI: 10.1021/acscatal.5b00495
ACS Catal. 2015, 5, 3995−4002

imately 10−20 nm, as shown Figure 1, it is believed that the effect of particle size on the ORR activity is negligible. In a recent study involving the $Ag/Mn_3O_4/C$ catalyst, a support with a Mn oxide/carbon mass ratio of 1:3 was prepared to induce high Ag particle dispersion in the oxides.[21] However, it was not possible to gain a clear understanding of the effect of the interactions between the metal and metal oxides on the ORR activity in that study, because Ag particles can be supported on carbon supports as well as oxide particles. Therefore, the amount of carbon on the surface was minimized in this study by employing a Mn_3O_4/carbon mass ratio of 5:1. To identify the distribution of each element, we performed element mapping analysis on the $Ag/Mn_3O_4/C$ catalyst. As shown in Figure S1, Mn_3O_4 were dispersed almost everywhere on catalysts and Ag nanoparticles were also covered uniformly on catalysts. Carbon mapping is not shown here as we used carbon grid for performing TEM analysis. As a result, most of the Ag particles are likely to be supported on Mn_3O_4, and the effect of the interactions between Ag and Mn_3O_4 on the ORR activity can be more accurately studied.

The crystal structures of the Ag particles and Mn_3O_4/C supports were examined by measuring the XRD patterns. Figure 2 presents the XRD patterns of Mn_3O_4/C, $Ag/Mn_3O_4/C$, and Ag/C. Mn_3O_4 was successfully synthesized as a single phase and its XRD pattern matched well with that of a typical tetragonal structure (S.G.141, I41/amdS) with no additional peaks.[40] On the other hand, Mn_3O_4 had a distorted spinel structure, owing to the Jahn−Teller effect. In this structure, Mn^{2+} occupies the tetrahedral sites, whereas Mn^{3+} occupies the octahedral sites.[41] The crystal structure of Ag supported on Mn_3O_4/C and carbon matched exactly with that of the face-centered cubic (fcc) structure (2θ = 38.3°, 44.2°, 64.4°, and 77.4°, corresponding to the (111), (200), (220), and (311) facets, respectively). The results indicated that the Ag particles were supported well on Mn_3O_4/C.

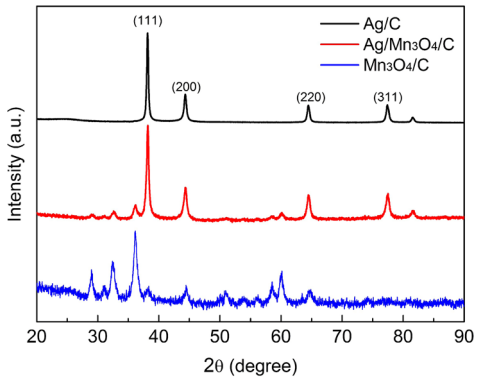

Figure 2. XRD patterns of Ag/C, $Ag/Mn_3O_4/C$, and Mn_3O_4/C.

Electrochemical Measurements. Figure 3a shows the CV curves of $Ag/Mn_3O_4/C$ and Ag/C in N_2 atmosphere. During the oxidation of Ag, a monolayer of Ag_2O is formed on the surface, whereas AgOH and Ag_2O are formed in the bulk. The Ag oxidation peak potential observed in the CV curve of Ag/C matched the value reported in the literature. In the case of $Ag/Mn_3O_4/C$, redox peaks of Ag and Mn were observed and the transitions from $Mn(OH)_2$ to Mn_2O_3 and MnOOH were reported to occur at approximately 0.7 and 0.86 V (vs RHE), respectively.[21] The peak starting at about 1.09 V (vs RHE) corresponded to the oxidation of MnOOH to MnO_2 and overlapped with the oxidation peak of Ag in this case. Therefore, it was difficult to identify the starting potential of the Ag oxidation peak in the CV curves of $Ag/Mn_3O_4/C$ and Ag/C. However, from the AgO reduction peaks, it was confirmed that the AgO reduction reaction in $Ag/Mn_3O_4/C$ was much faster than that in Ag/C, based on the fact that the AgO reduction peak started earlier in the case of $Ag/Mn_3O_4/C$ compared to Ag/C. Fast reduction of the Ag surface is believed to be favorable for enhancing the ORR activity. Figure 3b shows the CV curves of $Ag/Mn_3O_4/C$ and Ag/C in O_2 atmosphere. Comparing with the CV curve in N_2 atmosphere, CV curve in O_2 atmosphere for $Ag/Mn_3O_4/C$ shows relatively broad anodic peaks of Mn oxide from 0.92 to 1.32 V, indicating absorption of OH^- at the surface as reported previously.[20] The peak from 0.72 to 0.92 V in cathodic curve corresponds to the ORR reaction which is shown at high potential for $Ag/Mn_3O_4/C$ than that for Ag/C, suggesting that oxygen reduction reaction for $Ag/Mn_3O_4/C$ is faster than that for Ag/C.

The ORR activity was examined using a thin-film rotating disk electrode (TFRDE) technique.[36] As shown in Figure 4, the ORR activity for $Ag/Mn_3O_4/C$ measured at 1600 rpm was significantly higher than that of Ag/C. In contrast, the onset potential for the ORR in the case of Ag/C was approximately 0.82 V (vs RHE), which matches well with the previously reported data.[18] The onset potential for the ORR in the case of $Ag/Mn_3O_4/C$ was approximately 0.92 V (vs RHE), which is close to the ORR onset potential observed in the case of Pt/C. In the literature, the onset potential for the ORR in the case of AgCo alloy (0.77 V), $LaCu_{0.5}Mn_{0.5}O_3$ (0.8 V), Ag−Mn oxide

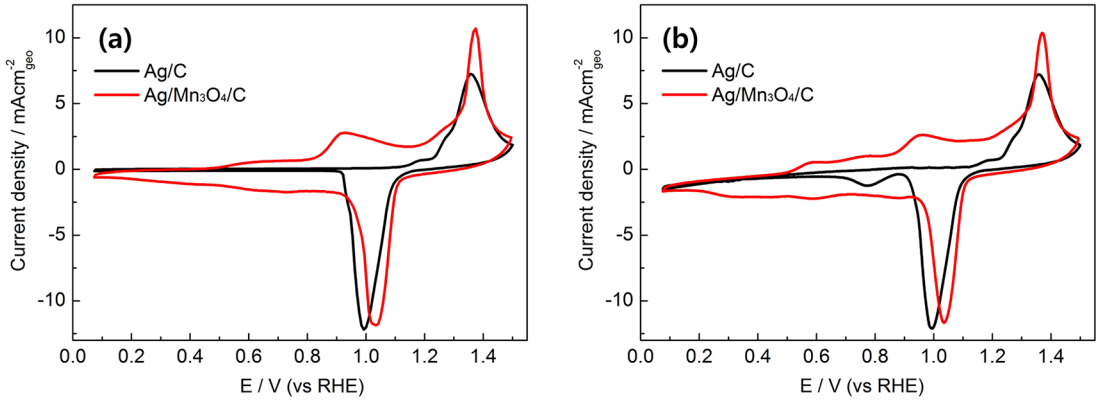

Figure 3. Cyclic voltammetry of Ag/C and $Ag/Mn_3O_4/C$ catalysts (a) in N_2-saturated and (b) in O_2-saturated 0.1 M KOH at 20 mV s^{-1}.

DOI: 10.1021/acscatal.5b00495
ACS Catal. 2015, 5, 3995−4002

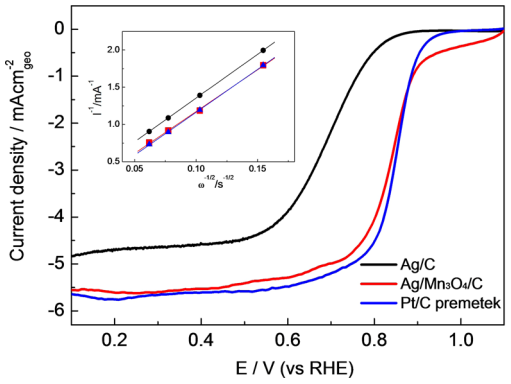

Figure 4. Oxygen reduction polarization curves for Ag/C, Ag/Mn_3O_4/C, and Pt/C premetek at 1600 rpm in O_2-saturated 0.1 M KOH at 10 mV s^{-1}. (inset) Koutecky–Levich plots for ORR in the presence of Ag/C, Ag/Mn_3O_4/C, and Pt/C premetek at 0.32 V vs RHE.

composites on carbon (0.84 V), Co_3O_4 nanocrystals on graphene (0.85 V), and nitrogen doped graphene (approaching that of Pt/C) were reported.[12,21,42−44] Therefore, it is confirmed that the ORR activity of Ag/Mn_3O_4/C represents high electrocataytic performance.

Tafel plots derived from Figure 4 are shown in Figure S2 for Pt/C, Ag/Mn_3O_4/C, and Ag/C. For Ag/Mn_3O_4/C, the Tafel slope is close to 119 mV dec^{-1} at the high overpotentials, but the slope at the low overpotentials is hardly discovered because of the capacitance of Mn oxide. For a Pt/C, the Tafel slopes were reported to be about 60 and 120 mV dec^{-1} at low and high overpotentials, reperesenting the rate-determining step of a one-electron transfer reaction and a two-electron transfer reaction, respectively.[45] The comparable Tafel slopes between the Ag/Mn_3O_4/C and Pt/C catalysts indicate that remarkable electrocataytic performance of the ORR for Ag/Mn_3O_4/C in alkaline media.

In particular, the limiting current in the case of Ag/Mn_3O_4/C in Figure 4 was approximately 5.5 mA cm_{geo}^{-2}, which is close to the value for Pt/C (5.62 mA cm_{geo}^{-2}) and to the 4-electron pathway for the ORR. However, owing to the formation of peroxide in most of the ORRs, the limiting current for Ag/C was less than 5 mA cm_{geo}^{-2}, indicating a pseudo 4-electron pathway (2-electron pathway or 4-electron pathway). To calculate the electron transfer number in the ORR, the Levich plot obtained using the Koutecky–Levich equation[45] is presented in the inset of Figure 4.

$$I_{lim} = 0.62nFAD^{2/3}\nu^{-1/6}C_0\omega^{1/2} \quad (1)$$

In the above equation, I_{lim} is the limiting current density, n is the number of electrons transferred per oxygen molecule, F is the Faraday's constant (F = 96485.3399 C mol^{-1}), A is the geometric area of the electrode (A = 0.19625 cm^2), D is the diffusion coefficient of oxygen in 0.1 M KOH ($D = 1.9 \times 10^{-5}$ cm^2 s^{-1}), ν is the kinematic viscosity ($\nu = 1.1 \times 10^{-2}$ cm^2 s^{-1}), C_0 is the oxygen concentration ($C_0 = 1.2 \times 10^{-6}$ mol cm^{-3}), and ω is the rotation speed in radians. It is well-known that the electrochemical reduction of O_2 can occur via two pathways, namely a two-electron pathway to produce HO_2^- and a four-electron pathway to produce H_2O. It is also agreed that the ORR in Pt/C occurs via the four-electron pathway, resulting in the direct production of H_2O. The electron transfer number for Ag/C calculated from the Koutecky–Levich equation was approximately 3.71, whereas the electron transfer number for Ag/Mn_3O_4/C was approximately 3.98, indicating an exclusive four-electron pathway in the latter case.

To verify the electron transfer number of catalysts, we performed rotating ring-disk electrode (RRDE) measurements to monitor the formation of peroxide species during the ORR process for Ag/Mn_3O_4/C and Ag/C. As shown in Figure 5, ring current of peroxide oxidation for Ag/Mn_3O_4/C obviously decreased than that for Ag/C, indicating that peroxide formation (two-electron pathway) for Ag/Mn_3O_4/C was

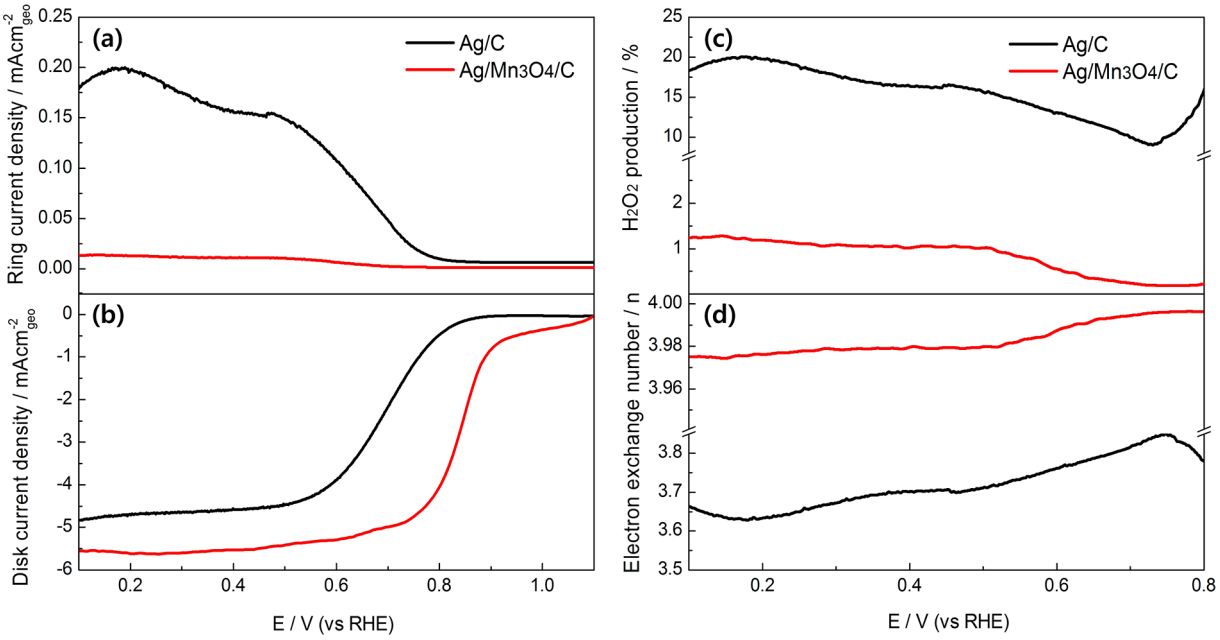

Figure 5. (a) The ring current densities, (b) the disk current densities, (c) H_2O_2 yields, and (d) electron exchange number during the RRDE measurements of the ORR on the Ag/C and Ag/Mn_3O_4/C catalysts with a rotation rate of 1600 rpm in a 0.1 M KOH solution. Collection efficiency N = 0.38; the ring potential E_{ring} = 1.26 V; scan rate = 10 mV s^{-1}.

DOI: 10.1021/acscatal.5b00495
ACS Catal. 2015, 5, 3995−4002

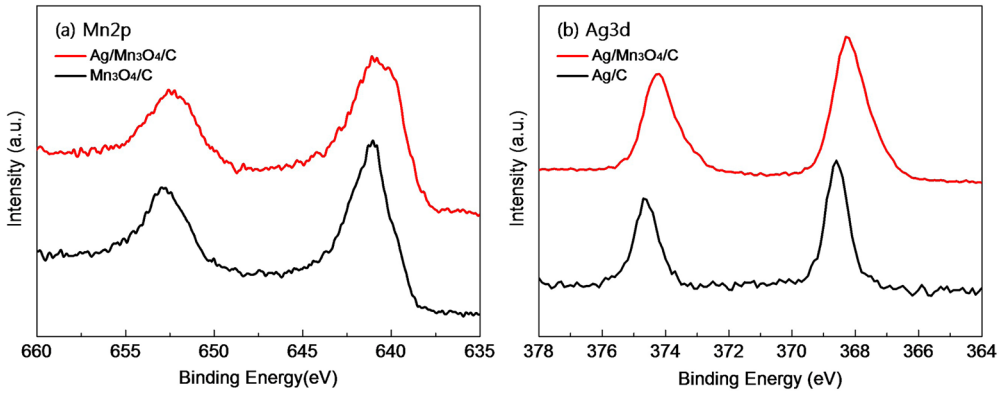

Figure 6. (a) Mn 2p XPS spectra for $Ag/Mn_3O_4/C$ and Mn_3O_4/C and (b) Ag 3d XPS spectra for $Ag/Mn_3O_4/C$ and Ag/C.

reduced. As shown in Figure 5c and d, the electron transfer number for $Ag/Mn_3O_4/C$ and Ag/C were clearly confirmed by calculated percentage of peroxide production.[21] The electron exchange number on the $Ag/Mn_3O_4/C$ is about 3.98 and that on the Ag/C is about 3.7, which agrees well with the value calculated by Koutecky–Levich equation. Therefore, it is confirmed that the ORR activity of $Ag/Mn_3O_4/C$ is significantly higher than that of Ag/C.

Since specific activity is dependent on the active site area, the electrochemical active surface areas (ECSA) of the catalysts were compared. The ECSAs of the catalysts were determined using the AgO reduction peak in the CV. The AgO reduction peak charges for $Ag/Mn_3O_4/C$ and Ag/C were 58.8 and 59.3 mC cm_{geo}^{-2}, respectively. It may be noted that the capacitance of Mn_3O_4 is added to the AgO reduction peak in the case of $Ag/Mn_3O_4/C$. Therefore, it can be concluded that since Ag/C has more active sites than $Ag/Mn_3O_4/C$, the ORR activity is likely to be higher in the case of the former compared to the latter. However, as evident from the ORR polarization curves, $Ag/Mn_3O_4/C$ exhibited a rather higher ORR activity compared to Ag/C, implying that the size alone cannot be used as a reasonable indicator for assessing the enhancement in the ORR activity in this case.

The rate equation for the ORR can be given by eq 2, using the Butler–Volmer equation, which is a basic equation in electrochemistry that relates kinetic current i and potential E.[46]

$$i = nFKc_{O2}(1 - \theta_{ad})^{x}\exp(-\beta FE/RT)\exp(-\gamma \Delta G_{ad}/RT) \quad (2)$$

In the above equation, i is the measured current density, n is the number of electrons, K is the rate constant, x is the order of active sites, β and γ are symmetry factors (assumed to be 1/2), R is the universal gas constant, T is the temperature, c_{O2} is the concentration of O_2, θ_{ad} is the total surface coverage by the adsorbed spectator species, and G_{ad} is the Gibbs free energy of the reaction intermediates. Among the variables in the above equation, the key parameter that determines the ORR kinetics is the $(1 - \theta_{ad})$ term, because the number of active sites for the ORR depends on the OH coverage on the surface. Therefore, examination of the O–O bond breakage and adsorption strength of O_2 on the electrochemical catalysts is necessary, because the OH surface coverage depends on the adsorption of the oxygen species. Therefore, two important electronic effects that determine the ORR activity, namely the ligand and strain effects, were investigated in this study, to comprehensively understand the basic principles involved in the enhanced ORR activity achieved by using $Ag/Mn_3O_4/C$ as a catalyst.

DISCUSSION

Ligand Effect. The adsorption strength of the oxygen species on the surface of an electrochemical catalyst and the electronic effect that directly induces O–O bond breakage are believed to be the main factors that determine the ORR activity. There are two electronic effects, namely the ligand effect from charge transfer among the metal, promoter, and supports and the strain effect resulting from the lattice strain caused by the difference in the atomic radii or atomic interactions. To examine the change in the electronic structure of $Ag/Mn_3O_4/C$ in detail, XPS, XANES analysis from synchrotron beams, and DFT calculations were performed to study the ligand effect and EXAFS analysis was conducted to study the strain effect.

The XPS spectra of Mn 2p and Ag 3d core levels are presented in Figure 6. As shown in Figure 6a, the binding energies of the Mn $2p_{3/2}$ orbital for Mn_3O_4/C and $Ag/Mn_3O_4/C$ were 642.3 and 641.8 eV, respectively. The binding energy in the case of Mn_3O_4/C (641.3 eV) was between the values for Mn^{3+} (641.4 eV) and Mn^{2+}(641 eV) and matched well with the value reported in the literature (641.2 eV).[47] In contrast, the binding energy of the Mn $2p_{3/2}$ orbital for $Ag/Mn_3O_4/C$ (640.9 eV) was shifted to a lower energy compared to that of Mn_3O_4. As shown in Figure 6b, the binding energies of the Ag $3d_{5/2}$ orbital for Ag/C and $Ag/Mn_3O_4/C$ were 368.7 and 368.2 eV, respectively. The binding energy of Ag/C matched the value obtained in the metallic state (Ag^0), whereas the binding energy of $Ag/Mn_3O_4/C$ was red-shifted between Ag^0 (368.7 eV) and Ag^+ (367.6 eV).[47] The reduction of Mn and oxidation of Ag, after Ag was supported on Mn_3O_4/C, was caused by the charge transfer from Ag to Mn, owing to the difference in the work functions between Ag and Mn_3O_4. In general, Mn_3O_4 is a p-type semiconductor with a work function of 4.4 eV,[48,49] whereas Ag has a work function of 4.26 eV.[50] Therefore, charge transfer from Ag (with low work function) to Mn_3O_4 (with high work function), is likely to have occurred. Adzic et al. reported that the difference in ORR activity in alkaline media is related with a volcano plot due to the difference in O–O bond breaking and adsorption strength of O_2 depending on a d-band center of metal.[30] Metals with high d-band centers such as Ru, Ir, Rh, and Pd have low ORR activities, owing to difficulties in the desorption of oxygenated intermediates due to high adsorption strength of O_2, even though the O–O bonds are broken easily. On the other hand, metals with low d-band centers such as Ag and Au have low ORR activities, owing to the slow kinetics of the O–O bond breakage, even though O_2

DOI: 10.1021/acscatal.5b00495
ACS Catal. 2015, 5, 3995–4002

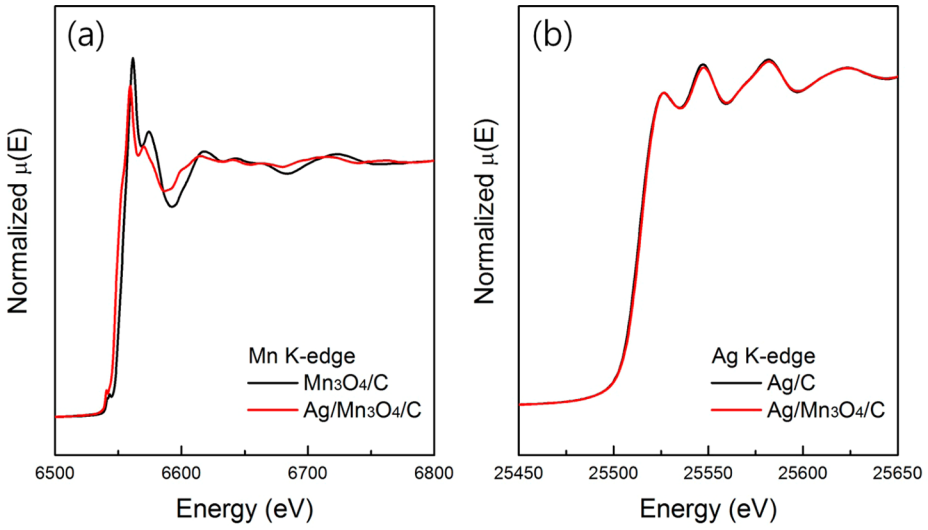

Figure 7. (a) Mn *k*-edge XANES spectra for $Ag/Mn_3O_4/C$ and Mn_3O_4/C and (b) Ag *k*-edge XANES spectra for $Ag/Mn_3O_4/C$ and Ag/C.

adsorption is sufficiently weak. Therefore, enhancing the kinetics of the O−O bond breakage by raising the d-band center is crucial, to maximize the ORR activity of Ag. The XPS results for the $Ag/Mn_3O_4/C$ catalyst showed a d-band vacancy for Ag, owing to the charge transfer from Ag to Mn. This is expected to favor the O−O bond split during the ORR.

Figure 7 shows the measured XANES spectra, which can predict the change in the electron density accurately. Figure 7a shows the Mn *k*-edge XANES spectra of $Ag/Mn_3O_4/C$ and Mn_3O_4/C. In the k-edge spectrum, a p-band vacancy was observed because a core electron was excited from the 1s orbital to the continuum state. The XANES edge of $Ag/Mn_3O_4/C$ was shifted to a lower energy compared to Mn_3O_4/C and a reduction of the white line was observed. This confirms the reduction of Mn in $Ag/Mn_3O_4/C$. Therefore, as indicated by the XPS results, electron acceptance by Mn as a result of charge transfer was confirmed. Figure 7b shows the Ag *k*-edge XANES spectra for $Ag/Mn_3O_4/C$ and Ag/C. Although the XPS results suggested that Ag is oxidized in the case of $Ag/Mn_3O_4/C$, the XANES spectra of $Ag/Mn_3O_4/C$ and Ag/C showed little difference. Therefore, it is highly likely that charge transfer mainly happened in the d-band because the white line of the Ag XANES spectrum showed little change in the p-band. In addition, it is surmised that charge transfer, which occurred locally at the Ag/Mn interface, could not be observed because the XANES data was obtained in the transmission mode.

Although the XPS and XANES measurements can provide some evidence of charge transfer, in-depth information on the electron population of each orbital or electron structure such as the total charge of each component cannot be obtained. Therefore, DFT calculations using plane-wave expansion of the wave functions and CASTEP code of the Vanderbilt-type ultra pseudopotential formalism[39,38] were employed in this study. Table 1 presents the calculated Mulliken electronic populations and total charge of Mn_3O_4/C, $Ag/Mn_3O_4/C$, and Ag/C. The charge of Mn in $Ag/Mn_3O_4/C$ was more reduced compared to Mn_3O_4/C, whereas the charge of Ag in Mn_3O_4/C was similar to that in carbon. On the other hand, reduction of d-band electrons was observed. It is believed that charge was transferred to Mn in the d-band rather than in the sp-band of Ag, because difference in Ag charge was mainly observed in the d-band in the DFT calculation results. The electron

Table 1. Occupied States in the s, p, d, and f Orbitals and the Calculated Charge Transfer in Mn_3O_4/C, $Ag/Mn_3O_4/C$, and Ag/C

	s	p	d	f	charge
O	1.860	4.700	0	0	−0.550
Mn	0.270	0.400	5.633	0	0.734
O	1.882	4.632	0	0	−0.515
Mn	0.420	0.316	5.666	0	0.596
Ag	0.812	0.266	9.868	0	0.050
C	1.186	2.816	0	0	−0.006
Ag	0.873	0.080	9.983	0	0.060

densities of states of $Ag/Mn_3O_4/C$ and Ag/C obtained from the DFT calculations were studied to examine the change in the d-band center of Ag, as shown in Figure 8. The d-band centers

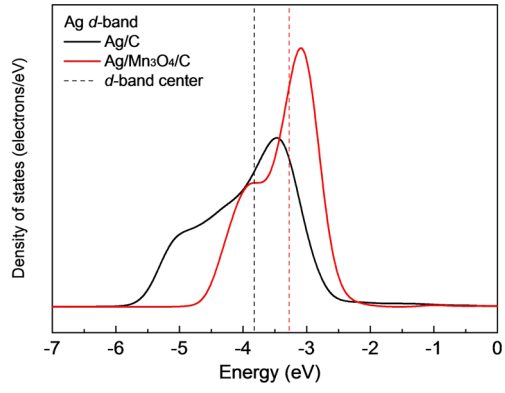

Figure 8. Calculated d-band electron densities for Ag/C and $Ag/Mn_3O_4/C$. Dashed lines represent the d-band center positions.

of $Ag/Mn_3O_4/C$ and Ag/C were at −3.276 and −3.825 eV, respectively. The higher d-band center obtained in the case of $Ag/Mn_3O_4/C$ compared to Ag/C was due to the oxidation of Ag. This result is in a good agreement with the tendency of the d-band to turn sharp, owing to the reduction of the d-band superposition, resulting in an increase in the d-band center when an electron is lost from the d-band.[51,52] So far, the weak O−O bond split on the surface of the Ag metal was unfavorable for promoting ORR activity.[30] However, an apparent increase

DOI: 10.1021/acscatal.5b00495
ACS Catal. 2015, 5, 3995−4002

in the d-band vacancy in $Ag/Mn_3O_4/C$ can enhance the ORR activity by increasing the kinetics of the O−O bond breakage in the ORR.

Strain Effect. Lattice strain coupled with charge transfer can induce a significant change in the electronic structure. To investigate the lattice strain in $Ag/Mn_3O_4/C$, EXAFS analysis was employed in this study. EXAFS is a useful tool for understanding the microstructures in the lattice. Figure 9 and

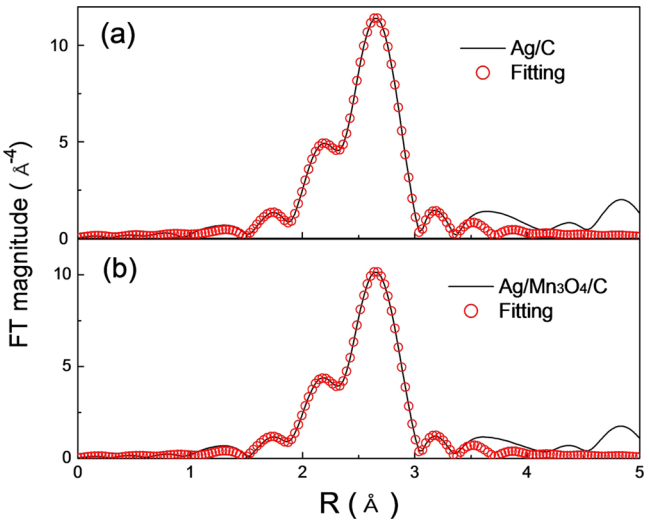

Figure 9. Fourier transforms of the EXAFS spectra at the Ag k-edge for (a) Ag/C and (b) $Ag/Mn_3O_4/C$.

Table 2. Curve-fitting Results for the EXAFS Data at the Ag *k*-Edge for Ag/C and $Ag/Mn_3O_4/C$ Catalysts

	shell	N	R (Å)	σ^2 (Å)
Ag/C	Ag−Ag	10.41	2.86(1)	0.01
$Ag/Mn_3O_4/C$	Ag−Ag	9.69	2.87(1)	0.01

Table 2 show the Fourier-transformed radial distribution function and a theoretical model calculated from the FEFF8.3 code for $Ag/Mn_3O_4/C$ and Ag/C. The calculated bond lengths of 1NN Ag−Ag in $Ag/Mn_3O_4/C$ and Ag/C were 2.87 and 2.86 Å, respectively. It is interesting that the Ag−Ag bond length in $Ag/Mn_3O_4/C$ was slightly higher than that in Ag/C. It is well-known from a report by Norskov et al. that an increase in bond length is caused by tensile strain in the lattice.[53] When there is tensile strain, an increase in the d-band center is expected because the d-band turns sharp, owing to the reduction in the d-band superposition. The increase in the d-band center of Ag in the volcano plot reported by Adzic et al. is thought to enhance the kinetics of the O−O bond split, resulting in favorable ORR activity. Therefore, based on the calculated lattice strain, it is believed that the strain effect in addition to the ligand effect is also favorable for promoting the ORR activity.

CONCLUSION

In this study, we investigated the electronic effect between Ag and Mn_3O_4 on the ORR activity in alkaline media. Ag supported on Mn_3O_4/C showed a significantly enhanced ORR activity compared to Ag supported on carbon. To understand the cause for the activity enhancement, we thoroughly examined two major effects, namely the ligand and strain effects. In the case of the ligand effect, the charge transfer from Ag to Mn increased the d-band vacancy and kinetics of the O−O bond split, resulting in favorable ORR activity. Further, in the case of the strain effect as determined from the EXAFS analysis, the shift in the d-center increased the kinetics of the O−O bond split and resulted in ORR activity enhancement for $Ag/Mn_3O_4/C$. Therefore, we propose that electronic effects need to be investigated when new metal/metal oxide catalysts are designed for enhancing ORR activity in alkaline media.

ASSOCIATED CONTENT

Supporting Information

The Supporting Information is available free of charge on the ACS Publications website at DOI: 10.1021/acscatal.5b00495.

TEM-EDS and Tafel plot (PDF)

AUTHOR INFORMATION

Corresponding Author

*E-mail: yongtae@pusan.ac.kr.

Notes

The authors declare no competing financial interest.

ACKNOWLEDGMENTS

This work was supported by the National Research Foundation of Korea (NRF) grant (2013M1A8A1040703) and GCRC-SOP funded by the Korea government (MEST). We thank Dr. Hannah Song and Dr. Eun-Kyung Lee for fruitful discussion.

REFERENCES

(1) Neburchilov, V.; Wang, H. J.; Martin, J. J.; Qu, W. *J. Power Sources* **2010**, *195*, 1271−1291.
(2) Tan, C.; Wang, F.; Liu, J. J.; Zhao, Y. B.; Wang, J. J.; Zhang, L. H.; Park, K. C.; Endo, M. *Mater. Lett.* **2009**, *63*, 969−971.
(3) Demarconnay, L.; Coutanceau, C.; Leger, J. M. *Electrochim. Acta* **2004**, *49*, 4513−4521.
(4) El-Deab, M. S.; Sotomura, T.; Ohsaka, T. *Electrochim. Acta* **2006**, *52*, 1792−1798.
(5) El-Deab, M. S.; Sotomura, T.; Ohsaka, T. *Electrochem. Commun.* **2005**, *7*, 29−34.
(6) Jiang, L.; Hsu, A.; Chu, D.; Chen, R. *J. Electrochem. Soc.* **2009**, *156*, B643−B649.
(7) Yang, Y. F.; Zhou, Y. H.; Cha, C. S. *Electrochim. Acta* **1995**, *40*, 2579−2586.
(8) Asazawa, K.; Sakamoto, T.; Yamaguchi, S.; Yamada, K.; Fujikawa, H.; Tanaka, H.; Oguro, K. *J. Electrochem. Soc.* **2009**, *156*, B509−B512.
(9) Roche, I.; Chainet, E.; Chatenet, M.; Vondrak, J. *J. Phys. Chem. C* **2007**, *111*, 1434−1443.
(10) Matsuki, K.; Kamada, H. *Electrochim. Acta* **1986**, *31*, 13−18.
(11) Rios, E.; Gautier, J. L.; Poillerat, G.; Chartier, P. *Electrochim. Acta* **1998**, *44*, 1491−1497.
(12) Suntivich, J.; Gasteiger, H. A.; Yabuuchi, N.; Nakanishi, H.; Goodenough, J. B.; Shao-Horn, Y. *Nat. Chem.* **2011**, *3*, 546−550.
(13) Duan, J.; Chen, S.; Dai, S.; Qiao, S. Z. *Adv. Funct. Mater.* **2014**, *24*, 2072−2078.
(14) Liang, J.; Zhou, R. F.; Chen, X. M.; Tang, Y. H.; Qiao, S. Z. *Adv. Mater.* **2014**, *26*, 6074−6079.
(15) Ma, T. Y.; Dai, S.; Jaroniec, M.; Qiao, S. Z. *J. Am. Chem. Soc.* **2014**, *136*, 13925−13931.
(16) Zhou, R.; Qiao, S. Z. *Chem. Mater.* **2014**, *26*, 5868−5873.
(17) Han, J. J.; Li, N.; Zhang, T. Y. *J. Power Sources* **2009**, *193*, 885−889.
(18) Guo, J. S.; Hsu, A.; Chu, D.; Chen, R. R. *J. Phys. Chem. C* **2010**, *114*, 4324−4330.

DOI: 10.1021/acscatal.5b00495
ACS Catal. 2015, 5, 3995−4002

(19) Slanac, D. A.; Hardin, W. G.; Johnston, K. P.; Stevenson, K. J. *J. Am. Chem. Soc.* **2012**, *134*, 9812−9819.
(20) Slanac, D. A.; Lie, A.; Paulson, J. A.; Stevenson, K. J.; Johnston, K. P. *J. Phys. Chem. C* **2012**, *116*, 11032−11039.
(21) Tang, Q. E.; Jiang, L. H.; Qi, J.; Jiang, Q.; Wang, S. L.; Sun, G. Q. *Appl. Catal., B* **2011**, *104*, 337−345.
(22) Boskovic, I.; Mentus, S. V.; Pjescic, M. *Electrochim. Acta* **2006**, *51*, 2793−2799.
(23) Kim, J.-H.; Chang, S.; Kim, Y.-T. *Appl. Catal., B* **2014**, *158*, 112−118.
(24) Kim, J.-H.; Kwon, G.; Chun, H.; Kim, Y.-T. *ChemCatChem* **2014**, *6*, 3239−3245.
(25) Boskovic, I.; Mentus, S. V.; Pjescic, J. M. *Electrochem. Commun.* **2005**, *7*, 797−802.
(26) Han, X.; Cheng, F.; Zhang, T.; Yang, J.; Hu, Y.; Chen, J. *Adv. Mater.* **2014**, *26*, 2047−2051.
(27) Jasin, D.; Abu-Rabi, A.; Mentus, S.; Jovanovic, D. *Electrochim. Acta* **2007**, *52*, 4581−4588.
(28) Maheswari, S.; Sridhar, P.; Pitchumani, S. *Electrochem. Commun.* **2013**, *26*, 97−100.
(29) Mentus, S.; Abu Rabi, A.; Jasin, D. *Electrochim. Acta* **2012**, *69*, 174−180.
(30) Lima, F. H. B.; Zhang, J.; Shao, M. H.; Sasaki, K.; Vukmirovic, M. B.; Ticianelli, E. A.; Adzic, R. R. *J. Phys. Chem. C* **2007**, *111*, 404−410.
(31) Zeng, J. H.; Yang, J.; Lee, J. Y.; Zhou, W. J. *J. Phys. Chem. B* **2006**, *110*, 24606−24611.
(32) Newville, M. *J. Synchrotron Radiat.* **2001**, *8*, 322−324.
(33) Ravel, B. *J. Synchrotron Radiat.* **2001**, *8*, 314−316.
(34) Ravel, B.; Newville, M. *J. Synchrotron Radiat.* **2005**, *12*, 537−541.
(35) Newville, M. *J. Synchrotron Radiat.* **2001**, *8*, 96−100.
(36) Suntivich, J.; Gasteiger, H. A.; Yabuuchi, N.; Shao-Horn, Y. *J. Electrochem. Soc.* **2010**, *157*, B1263−B1268.
(37) Garsany, Y.; Baturina, O. A.; Swider-Lyons, K. E.; Kocha, S. S. *Anal. Chem.* **2010**, *82*, 6321−6328.
(38) Segall, M. D.; Lindan, P. J. D.; Probert, M. J.; Pickard, C. J.; Hasnip, P. J.; Clark, S. J.; Payne, M. C. *J. Phys.: Condens. Matter* **2002**, *14*, 2717−2744.
(39) Vanderbilt, D. *Phys. Rev. B: Condens. Matter Mater. Phys.* **1990**, *41*, 7892−7895.
(40) Boucher, B.; Buhl, R.; Perrin, M. *J. Phys. Chem. Solids* **1971**, *32*, 2429−2437.
(41) Tackett, R.; Lawes, G.; Melot, B. C.; Grossman, M.; Toberer, E. S.; Seshadri, R. *Phys. Rev. B: Condens. Matter Mater. Phys.* **2007**, *76*, 024409.
(42) Holewinski, A.; Idrobo, J.-C.; Linic, S. *Nat. Chem.* **2014**, *6*, 828−834.
(43) Liang, Y.; Li, Y.; Wang, H.; Zhou, J.; Wang, J.; Regier, T.; Dai, H. *Nat. Mater.* **2011**, *10*, 780−786.
(44) Geng, D.; Chen, Y.; Chen, Y.; Li, Y.; Li, R.; Sun, X.; Ye, S.; Knights, S. *Energy Environ. Sci.* **2011**, *4*, 760−764.
(45) Bard, A. J.; Faulkner, L. R. *Electrochemical methods: fundamentals and applications*, 2nd ed.; Wiley: New York, 2001.
(46) Stamenkovic, V. R.; Fowler, B.; Mun, B. S.; Wang, G. F.; Ross, P. N.; Lucas, C. A.; Markovic, N. M. *Science* **2007**, *315*, 493−497.
(47) Briggs, D.; Seah, M. P. *Practical surface analysis*, 2nd ed.; Wiley: Chichester, 1990.
(48) Maniak, G.; Stelmachowski, P.; Zasada, F.; Piskorz, W.; Kotarba, A.; Sojka, Z. *Catal. Today* **2011**, *176*, 369−372.
(49) Na, C. W.; Park, S.-Y.; Chung, J.-H.; Lee, J.-H. *ACS Appl. Mater. Interfaces* **2012**, *4*, 6565−6572.
(50) Dweydari, A. W.; Mee, C. H. B. *physica status solidi(a)* **1975**, *27*, 223−230.
(51) Norskov, J. K.; Rossmeisl, J.; Logadottir, A.; Lindqvist, L.; Kitchin, J. R.; Bligaard, T.; Jonsson, H. *J. Phys. Chem. B* **2004**, *108*, 17886−17892.
(52) Xin, H. L.; Holewinski, A.; Schweitzer, N.; Nikolla, E.; Linic, S. *Top. Catal.* **2012**, *55*, 376−390.
(53) Shao, M. H.; Liu, P.; Zhang, J. L.; Adzic, R. *J. Phys. Chem. B* **2007**, *111*, 6772−6775.

DOI: 10.1021/acscatal.5b00495
ACS Catal. 2015, 5, 3995−4002